International Journal of Solids and Structures 50 (2013) 2078–2086

Contents lists available at SciVerse ScienceDirect

International Journal of Solids and Structures

journal homepage: www.elsevier.com/locate/ijsolstr

Analytical modeling to predict the cutting behavior of ferromagnetic steels: A coupled magnetic–mechanical approach

Ali Mkaddem [a,*], Abdelkader Benabou [b], Mohamed El Mansori [a], Stéphane Clénet [c]

[a] Arts et Métiers ParisTech, MSMP, Rue Saint Dominique B.P.508, 51006 Châlons-en-Champagne, France
[b] Universite de Lille 1, L2EP, Cité scientifique, 59655 Villeneuve-d'Ascq, France
[c] Arts et Métiers ParisTech, L2EP, 8 Boulevard Louis XIV, 59046 Lille Cedex, France

ARTICLE INFO

Article history:
Received 23 January 2012
Received in revised form 27 February 2013
Available online 30 March 2013

Keywords:
Dry cutting
Modeling
Magnetoplasticity
Dislocations
Shear bands
Friction

ABSTRACT

This paper discusses the reliability of a novel constitutive approach to model the magnetically assisted dry cutting of steel. The magnetic force combined with the mechanical force components, was found to be responsible for the perturbation observed in the primary shear angle. This perturbation is considered the basis of the analytical development. Quick-Stop Trials (QST) were first performed on AISI-1045 steel to investigate the shear angle evolution during the chip formation process. Both the Merchant and the Lee–Shaffer models were used to develop the coupled magnetic–mechanical approach. Magnetically free and magnetically assisted orthogonal cutting tests were then conducted to validate the analytical predictions. The shear angle showed a sensitive increase with the magnetic intensity until the steel magnetic saturation limit was reached. A magnetic field seems to be capable of altering the plastic shear, resulting in modification of the chip formation mechanisms. The neat drop observed in contact length proves the ability of the magnetic field to enhance the material flow along the secondary shear zone. The changes at the tool–steel interface, i.e., friction, are found to correlate strongly with the force magnitude change due to the magnetic component. The good agreement between the measurements and predictions demonstrates the efficiency of the proposed approach.

1. Introduction

For several years, the influence of a magnetic field on the mechanical behavior of ferromagnetic metals has been addressed. The phenomenon was initially indicated by Kravchenko (1970). He reported that magnetic excitations are capable of increasing the electron component of the viscous deceleration of dislocations to affect the plasticity in metals. The rearrangements within the microstructure ultimately affect the metal plasticity due to the collective motion of many dislocations (Balint et al., 2008). Several experiments have been conducted to prove the reliability of the theory describing the effects of magnetization on material properties (Galligan, 1982; Kim and Galligan, 1992). The change in plastic properties due to a magnetic field was attributed to the depinning of dislocations from obstacles. It was observed not only in very pure metals but also in any crystal materials such as semiconductors (Molotskii and Fleurov, 1996; Al'shits et al., 1994, 1997). The earlier verifications of the magnetization impacts on ferromagnetic bodies were performed by Molotskii and Fleurov (1997, 2000), who developed a basic magnetoplastic theory to explain the ability of a magnetic field to induce changes in the material plasticity. Multi-scale characterizations have been conducted to investigate the phenomenon. El Mansori et al. (1998) and El Mansori and Paulmier (1999) studied the role played by transferred layers in friction and wear in magnetized dry frictional applications. They explored the properties of the friction tracks in a steel–graphite couple to describe the wear mechanisms in ambient air and at room temperature. In the presence of active gases, they found that the magnetic field enhances carbon film transfer on the steel tracks. The carbon layer, which adheres well to the steel surface, leads to a significant reduction in friction and wear. However, in inert environments, the magnetic field favors the transfer of harder steel to softer graphite, thus generating an increase in friction and wear. Chin et al. (2001) investigated the tribological behavior and surface properties at interfaces of AISI-1045/AISI-1045 steel sliding contacts. Based on their experimental results, they concluded that the oxidation rate on a worn surface increases with magnetic intensity; hence, adhesion occurs, and local wear is consequently reduced at contact regions.

Bagchi and Ghosh (1971) studied the effects of a constant magnetic strength on tool wear when machining mild steel. In the range of speeds used, the authors found that tool wear decreases with the magnetic strength, while tool life depends on both the cutting speed and applied intensity. However, Singh et al. (2002) examined the surface finish after magnetically assisted abrasive

* Corresponding author. Tel.: +33 326699181; fax: +33 326699197.
E-mail address: ali.mkaddem@ensam.fr (A. Mkaddem).

0020-7683/$ - see front matter © 2013 Elsevier Ltd. All rights reserved.
http://dx.doi.org/10.1016/j.ijsolstr.2013.03.010

Nomenclature

B	magnetic induction B
f	feed rate
l_0	chip thickness in a magnetically free environment
r_0	chip compression ratio in a magnetically free environment
r_H	chip compression ratio in a magnetically assisted environment
F	resultant force of cutting in a magnetically free environment
F_{a0}	feed force in a magnetically free environment
F_{aH}	feed force in a magnetically assisted environment
F_{c0}	cutting force in a magnetically free environment
F_{cH}	cutting force in a magnetically assisted environment
F_H	resultant force of cutting in a magnetically assisted environment
F_m	magnetic force
H	magnetic intensity
V_c	cutting speed
Y_0	contact length between tool and chip in a magnetically free environment
Y_H	contact length between tool and chip in a magnetically assisted environment
φ_0	primary shear angle
φ_B	variation induced in the shear angle by the effect of magnetization
φ_H	total shear angle in a magnetically assisted environment
γ	rake angle
λ_0	friction angle
λ_B	partial quantity of friction angle due to a magnetic field
λ_H	total friction angle in a magnetically assisted environment
μ_B	Coulomb friction associated with the partial friction angle
$\mu_0^C l$	Coulomb friction coefficient
μ_H^{Cl}	Coulomb friction coefficient in a magnetically assisted environment
μ_0^{Tr}	Tresca friction coefficient
μ_H^{Tr}	Tresca friction coefficient in a magnetically assisted environment
ξ	stress distribution coefficient within the tool–material interface

flow machining. The authors showed that the surface roughness and material removal rate were improved by applying a magnetic field around the workpiece during machining. The research conducted on this topic (El Mansori et al., 2003, 2004; Åstrand et al., 2004; Chin et al., 2005) has been mainly focused on the 'qualitative' understanding of the physical changes arising from magnetization, whereas constitutive quantitative formulations are missing.

In recent decades, some attempts have been made to use external electromotive sources for improving the tribological conditions in dry cutting (Zaidi and Senouci, 1999) or in friction assemblies (El Mansori and Paulmier, 1999). These applications are not yet widely appreciated. In magnetically assisted cutting, an alternating or continuous magnetic field is essentially employed to rework the material at the moment of cutting or just before being cut. This procedure ensures minimum friction generation at the chip–tool interface and a high wear resistance of the cutting edge (Bataineh et al., 2003), which in turn improves the machinability of materials due to an improvement in plasticity. The mechanisms showing the benefits of magnetic assistance in the cutting process seem to be manifold (Jaspers and Dautzenberg, 2002a,b) and are basically separated into two subgroups: (i) the first is associated with the magnetically induced change in cutting mechanics; (ii) the second is much more associated with the tribological transformations involved under magnetization. To connect with the open literature, the development of a reliable plasticity model coupled with a magnetic field considers both. The first goal is to define the material behavior in a magnetized environment based on adequate assumptions, and the second aim is to avoid costly tests once the model is validated.

While the technological interest and experimental evidence of certain evoked mechanisms exist, the level of details provided remains insufficient for understanding the effects of magnetic assistance to cutting and as a basis for formulating process design rules. More specifically, the influence of a magnetic field on the evolution of mechanical or physical processes during ferromagnetic material cutting is not yet clear. Currently, it is very difficult to assess how the tool operates under such conditions. Through this attempt, one tries to partially address this issue.

In a magnetized environment, the magnetic force adds to the mechanical force components generated by the action of the cutting tool. The change involved in the force magnitudes results in a perturbation in the primary shear angle. Quick-stop machining tests were performed to investigate this perturbation in the chip formation process. Both the Merchant and Lee–Shaffer cutting models were used for developing the coupled magnetic–mechanical approach. Orthogonal tests were conducted using ranges of feed rates and cutting speeds to validate the approach. The effects of magnetization on tool–steel interface behavior are specifically discussed.

2. Cutting constitutive theories

2.1. Merchant model

Examining the surface plastic deformation mechanisms, e.g., shearing, has long attracted the attention of researchers. Understanding such mechanisms is a crucial step to improving the conditions of cutting, e.g., tool life, roughness of job surface, chip formation, etc. Modeling the cutting began with 2D analytical approaches and cutting applications were approximated by plane problems. Orthogonal cutting is the most used configuration in the open literature.

The model of Merchant (1945a,b) is based on perfect plastic behavior and a plane strain state. The thermal effects are neglected, and it primarily treats cutting problems with low speeds. The Merchant model assumes that the chip is essentially formed by simple shearing within a thin layer along a straight line OA starting at the tool-tip and inclined by the angle φ_0, as illustrated in Table 1. The formed chip slides against the rake face of the tool along the cutting length Y_0, and it flows along the rake face with a thickness l_0 that depends on the rake angle γ and, mostly, on the shearing mechanisms occurring within the contact zone OB, where local plastic deformation localizes and the secondary mechanisms of shearing develop. If one assumes that normal stress is uniformly distributed within the line OB, the contact length Y_0 (Table 1, Eq. (4a)) between the chip and the tool might be computed as a function of the shear angle φ_0 and the friction angle λ_0.

In the orthogonal cutting model, the compression ratio r_0 (Eq. (3a)) describing the chip flow of incompressible materials can be calculated from the feed rate and the chip thickness as $r_0 = f/l_0$.

Table 1
Constitutive equations of basic models of Merchant and Lee–Shaffer.

Model	Characteristic variables		Constitutive equations	
Merchant 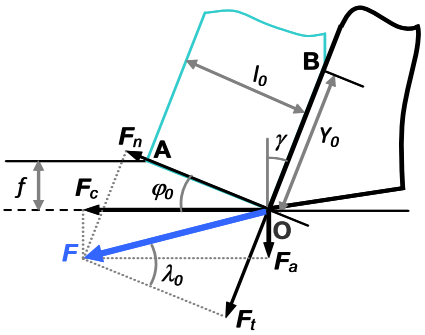	Shear angle	φ_0	$\frac{\pi}{4}-\frac{\lambda_0-\gamma}{2}$	(1a)
	Friction angle	λ_0	$2\left(\frac{\pi}{4}+\frac{\gamma}{2}\varphi_0\right)$	(2a)
	Compression ratio	r_0	$\frac{\sin\varphi_0}{\cos(\varphi_0-\gamma)}$	(3a)
	Contact length	Y_0	$\xi f.\frac{\sin(\varphi_0+\lambda_0-\gamma)}{\cos\varphi_0\cos\lambda_0}$	(4a)
	Coulomb criteria	μ_0^{Cl}	$\tan\lambda_0$	(5a)
	Tresca criteria	μ_0^{Tr}	$\frac{\sin(2\lambda_0)}{\cos(\lambda_0-\gamma)}$	(6a)
Lee–Shaffer 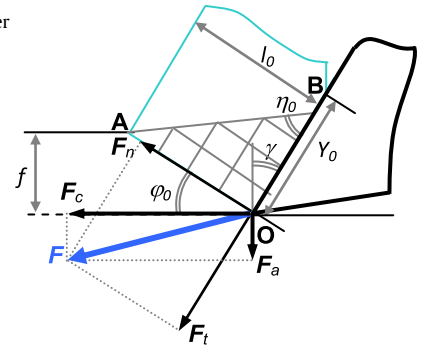	Shear angle	φ_0	$\frac{\pi}{4}-\lambda_0+\gamma$	(1b)
	Friction angle	λ_0	$\frac{\pi}{4}+\gamma-\varphi_0$	(2b)
	Compression ratio	r_0	$\frac{\sin\varphi_0}{\cos(\varphi_0-\gamma)}$	(3b)
	Contact length	Y_0	$\xi f.\frac{1}{\sqrt{2}\sin\varphi_0\cos\lambda_0}$	(4b)
	Coulomb criteria	μ_0^{Cl}	$\tan\lambda_0$	(5b)
	Tresca criteria	μ_0^{Tr}	$\sin 2\lambda_0$	(6b)

Increasing this ratio at a constant feed rate causes the chip thickness to decrease. On the one hand, this effect relies on the macroscopic material flow of the chip against the tool rake face. On the other hand, that effect is implicitly associated with the contact conditions at the interfaces OB, which are represented by the contact length Y_0 expressed in Eq. (4a). The coefficient ξ describes the stress state at the interface between the rake face and the material; ξ is 1 for a uniform distribution, 3/2 for a triangular decreasing distribution starting at the active point of the tool, and 9/7 for a constant trapezoidal distribution.

The primary shear angle, measured at the chip root, is defined so as to minimize the power provided to the system (tool-material). Under orthogonal dry cutting, generated interfaces between the tool and flow material are subjected to a severe surface-to-surface local pressure. This pressure results in friction rate depending on the angle λ_0. Based on this angle, the characteristic friction values at the interface OB could be estimated using the Coulomb (Eq. (5a)) and Tresca (Eq. (6a)) criteria.

2.2. Lee–Shaffer model

Lee and Shaffer (1951) developed their model using a slip lines approach. The slip lines field method is adapted for modeling plasticity problems during the plane strain state and non-hardening plastic behavior. In dry cutting, the region OAB is considered to be the active zone where the plastic flow criterion is reached. In that region, slip paths describe zones of equal shear stress. The model assumes that (i) stress is uniform within the region OAB delimited by the angles φ_0 and η_0, and (ii) the shear stress along OA is constant and it is related to the normal component along OB by the friction angle λ_0 (Tresca criteria). Finally, it assumes that (iii) the stress vector along AB is null. Therefore, beyond that line, the chip is formed freely. In the frame assumptions of the slip lines model, Eqs. (3b) and (4b) express the compression ratio and the contact length, respectively. The coefficient ξ was fixed to one for a uniform stress distribution within the contact region.

The expressions of r_0 are similar for the two models, but the angle φ_0 is identified differently. The Coulomb friction (Eq. (5b)) remains proportional to the angle λ_0. Moreover, the Tresca and Coulomb criteria can be connected in the following manner:

$$\frac{\mu_0^{Tr}}{\mu_0^{Cl}} = 2.\cos^2\lambda_0 \tag{7}$$

3. Coupled magnetic–mechanical approach

As mentioned in the basis theory of cutting, the shearing processes in the primary zone are the principal mechanisms that influence the formation of the chip and its morphology arising from the localized deformations along OB. Applying a magnetic field on the tool-steel pair induces changes in the properties of the cutting system; magnetic component F_m (Fig. 1c) emerges to be added to the mechanical components. In turn, this manifests through the perturbations involved in the primary shear zone.

Fig. 1d shows a representative configuration of the modification generated by the magnetic force. By taking these changes into account, a model can be developed. The usual equation connecting the cutting force/feed force ratio (F_{c0}/F_{a0}) to the shear angle (Merchant, 1945b; Lee and Shaffer, 1951) is given by the following equation:

$$\varphi_0 = \frac{1}{2}arctan\left(\frac{F_{c0}}{F_{a0}}\right) \tag{8}$$

In a magnetized environment, the above equation becomes the following equation:

$$\varphi_H = \frac{1}{2}arctan\left(\frac{F_{cH}}{F_{aH}}\right) \tag{9}$$

where the subscript 'H' refers to the non-zero magnetic intensity.

The chip roots experimental observations have demonstrated that in a magnetic field of intensity H, the shear angle changes

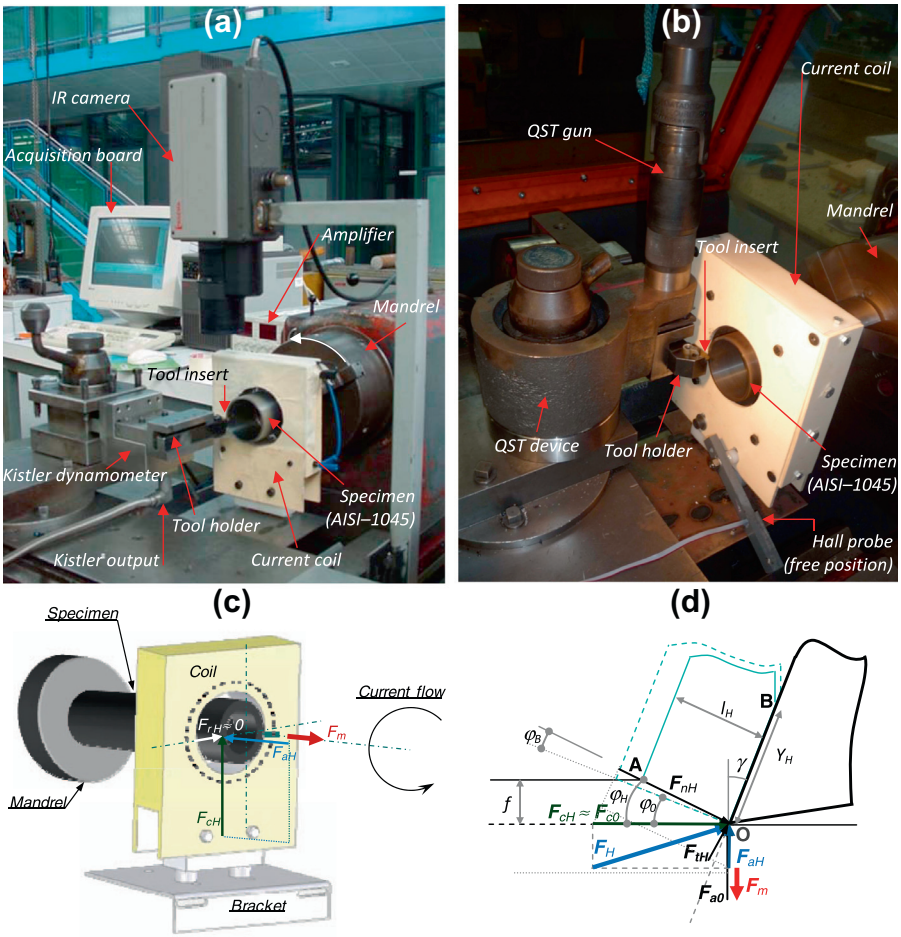

Fig. 1. Experimental set-up. (a) Continuous cutting test device, (b) Quick-Stop Test device, (c) Developed forces in magnetically assisted cutting, and, (d) Updated diagram of forces.

sensitively by a specified quantity to be denoted here as φ_B. Therefore, in a magnetic field, the shear angle might be modeled by the following form:

$$\varphi_H = \varphi_0 + \varphi_B(H) \tag{10}$$

where φ_B (algebraic quantity) is the magnetic field-dependent function that should be identified experimentally for each material. In the absence of a magnetic field, one assumes $\varphi_{H=0} = \varphi_0$. Otherwise, the equations of Table 1 should be rewritten for the coupled approach. To distinguish the magnetic field contribution to changing the material behavior when it is being cut, the coupled equations were written to produce the basic forms of the variables. In the presence of a field H, combining Eqs. (2a) and (2b) with Eq. (10) leads to the updated form of the friction angle:

$$\lambda_H = \lambda_0 - \lambda_B(H) \tag{11}$$

λ_B is an algebraic quantity representing the magnetically induced contribution to the friction angle. For Merchant and Lee–Shaffer, Eq. (11) takes the following forms, respectively:

$$\lambda_H = 2\left(\frac{\pi}{4} + \frac{\gamma}{2} - \varphi_H\right) = \lambda_0 - 2\varphi_B \tag{12a}$$

$$\lambda_H = \left(\frac{\pi}{4} + \gamma - \varphi_H\right) = \lambda_0 - \varphi_B \tag{12b}$$

The chip compression ratios of Eqs. (3a) and (3b) will be

$$r_H = r_0 \frac{\cos\varphi_B + \frac{\sin\varphi_B}{\tan\varphi_0}}{\cos\varphi_B - \sin\varphi_B.\tan(\varphi_0 - \gamma)};\ \varphi_B = \frac{\lambda_B}{2} \tag{13a}$$

$$r_H = r_0 \frac{\cos\varphi_B + \frac{\sin\varphi_B}{\tan\varphi_0}}{\cos\varphi_B - \sin\varphi_B.\tan(\varphi_0 - \gamma)};\ \varphi_B = \lambda_B \tag{13b}$$

Under the aforementioned assumptions and considering Eqs. (4a) and (4b), respectively, the calculation determines the contact length within the interface as

$$Y_H = Y_0.\frac{\cos\varphi_B - \sin\varphi_B\tan\varphi_0}{\left[\cos\varphi_B + \frac{\sin\varphi_B}{\tan\varphi_0}\right][\cos\lambda_B + \sin\lambda_B.\tan\lambda_0]} \tag{14a}$$

$$Y_H = Y_0.\frac{1}{\left[\cos\varphi_B + \frac{\sin\varphi_B}{\tan\varphi_0}\right][\cos\lambda_B + \sin\lambda_B.\tan\lambda_0]} \tag{14b}$$

Rewriting Eqs. (5a) and (5b) gives the updated forms of the friction coefficients according to the Coulomb criteria as described by Merchant and Lee–Shaffer, respectively:

$$\mu_H^{Cl} = \mu_0^{Cl}.\frac{1 - \frac{\mu_B}{\mu_0^{Cl}}}{1 + \mu_0^{Cl}.\mu_B};\ \mu_B = \tan\lambda_B = \tan 2\varphi_B \tag{15a}$$

$$\mu_H^{Cl} = \mu_0^{Cl}.\frac{1 - \frac{\mu_B}{\mu_0^{Cl}}}{1 + \mu_0^{Cl}.\mu_B};\ \mu_B = \tan\lambda_B = \tan\varphi_B \tag{15b}$$

Substituting the friction angle forms evaluated in magnetically assisted environments into Eqs. (6a) and (6b) leads to rewriting the

Tresca friction coefficient as described in the Merchant and Lee–Shaffer models, respectively:

$$\mu_H^{Tr} = \mu_0^{Tr} \cdot \frac{\cos 2\lambda_B - \frac{\sin 2\lambda_B}{\tan 2\lambda_0}}{\cos \lambda_B + \sin \lambda_B . \tan(\lambda_0 - \gamma)} \tag{16a}$$

$$\mu_H^{Tr} = \mu_0^{Tr} \cdot \left[\cos 2\lambda_B - \frac{\sin 2\lambda_B}{\tan 2\lambda_0}\right] \tag{16b}$$

4. Experimental details

The turning end of a tube arrangement is considered to perform orthogonal cutting tests on low-annealed AISI-1045 carbon steel. A specific device using a current excitation generator has been adopted to provide a magnetic field as the specimen translates in the cutting machine. The choice of such an alloy widely used in engineering practice relies on two arguments: the first is that it produces straight and continuous chips at low cutting speeds with obvious microstructure distinction; the second is that it is soft ferromagnetic steel that is easily magnetized. The material was annealed at 850 °C for 1 h and then stabilized at 600 °C for 1 h. This material is characterized by hard perlitic aggregates, a soft ferritic matrix, small grain size, tensile strength of 700 MPa, and an average micro-hardness at the annealed state of 225 ± 1.6 Hv. Table 2 summarizes the chemical composition of the steel used.

The magnetic field, crossing the specimen in the direction of the tool motion, was produced by an electric current coil fixed around the specimen (Fig. 1a). The coil is 110 mm in mean diameter and 40 mm in length. It is capable of providing a maximum magnetic intensity of 35 kA m^{-1}. An Allegro Hall probe was used for controlling the coil-delivered intensity during each test. Specimens are 64 mm in internal diameter, 3 mm in thickness, and 110 mm in length. To obtain reliable results, each series of tests was repeated five times under identical conditions, using a new insert edge for every test. The dry cutting tests (Table 3) were performed at room temperature using a tungsten carbide insert (TPUN-11-03-04-D) with 6° rake angle, 5° clearance angle, and 0.4 mm nose radius.

To investigate the material flow within the chip roots, quick-stop cutting tests were performed (Fig. 1b). After each test, the produced chip and the generated surface of the specimen were examined using optical microscopy. The microstructure of the AISI-1045 alloy was revealed by a chemical etching with 2% nital solution (2 ml HNO_3 and 98 ml ethanol) after a fine polishing with a 0.5 μm diamond suspension.

5. Results and discussion

5.1. Effectiveness of the proposed approach

The sensitivity of the primary shear angle to the magnetic intensity has been investigated on chip roots (e.g., Fig. 2a and b) obtained from quick-stop tests. Physically, the magnetization suppresses the Bloch walls in ferromagnetics, which favors the dislocation motion throughout the Weiss domains of the matrix material. This should alter the slip bands within the primary shear zone (Mkaddem and El Mansori, 2012) and, in many cases, might transform the chip morphology from segmental to continuous as observed in the micrographs of Fig. 2a and b.

The evolutions of the shear angle vs. magnetic intensity are given in Fig. 2c and d. It can be observed that the shear angle varies sensitively with the magnetic intensity. Three domains of variation can be distinguished. The first (I) corresponds to a sharp increase in the shear angle marked by a high slope characterizing the magneto-elastic steel behavior at relatively low intensity. The material reacts suddenly due to the magnetic shock, which physically results in high entropy and causes the depinning of free dislocations from weak obstacles. The first domain is followed by a transition zone (II); beyond that, the material reaches its magnetic saturation limit (III) from 8 kA m^{-1}.

The primary shear angle characterizes the straight zone between the cutter point and the free edge of the chip (Fig. 1d) when a cutting system operates. This zone is particularly specified by the discontinuity of the local tangential velocity field (Merchant, 1945a). The measurements conducted in the magnetic field showed that the shear angle at the saturation domain is approximately 3° higher than that obtained in the absence of a magnetic field. By Eq. (10), it follows that the magnetically generated angle φ_B is positive. Based on the inverse method, the experimental data were fitted using least square errors to obtain an analytical approximation. The type of approximation law was chosen so as (i) to generate the best fit to the experimental value and (ii) to minimize the number of constants to determine. The exponential law seems to be the most satisfactory form because it requires identifying only one parameter, i.e., the shear angle at saturation (φ_S). Hence, the variation of the shear angle vs. the magnetic field is given as

$$\varphi_H = \varphi_S - k_\varphi . e^{-\beta . f . H} \tag{17}$$

where φ_S is the shear angle at the magnetic saturation limit of the steel, $k\varphi = \varphi_S - \varphi_0$ at given conditions of cutting, and β (e.g., for AISI-1045, $\beta = 7$) is a material-dependent constant to determine experimentally from the magnetic behavior '$B = g(H)$' of the steel, where 'g' is an exponential function.

5.2. Interpretation of the analytical predictions

5.2.1. Contact length

From the mathematical point of view, Eqs. (14a) and 14b show that the contact length decreases when operating in a magnetically assisted environment, which results in a decrease in cutting time and, consequently, enhances the lifetime of cutting tools. The contact length was computed by referring to measured shear angle values, and the results were reported in Fig. 3a and b. As can be observed, the Merchant model leads to the highest variation between the magnetically free value and magnetically assisted value at the saturation domain regardless of the speed used. The variation is approximately three times lower when using the Lee–Shaffer model. The good agreement found between the results based on the

Table 2
Experimental details used for cutting tests.

Element	C	Si	S	Mn	P	Cr	Ni	Mo
Composition (%)	0.47	0.32	0.005	0.71	0.009	0.18	0.04	0.005

Table 3
Design of experiments considered for dry cutting tests.

Depth of cut (mm)	Feed rate (mm rev^{-1})	Speed (m min^{-1})	Magnetic intensity (kA m^{-1})
3	0.10	44	0–24
		138	0–24
	0.15	44	0–24
		138	0–24

measurements and the analytical predictions confirms the success of the coupled magnetic–mechanical formulation. Once the magnetic intensity reaches 8 kA m^{-1}, the curves based on the measurements as well as the predicted curves neatly stabilize irrespective of the conditions used. This effect was attributed to the magnetic saturation phenomenon taking place within the third domain (Fig. 2).

In any event, the behavior at the tool–chip interface must change in such a manner to decrease Y_H in a magnetically assisted environment. Thus, the time of contact between the tool and the secondary layer of produced chip drops. This ultimately delays the wear of the tool and, consequently, improves its lifetime.

The main interest in magnetically induced assistance arises from its ability to prevent the instability of deformation in the primary shear zone. If the cutting speed is high enough when dry turning steel, the magnetoplastic effect might reach such a level so as to control the cutting process stability. El Mansori and Mkaddem (2007) proved that a segmental chip obtained from a magnetically free cutting process transforms to a continuous chip when operating under magnetization. This action is extended to the secondary shear zone, where the deformation pattern is excessive and the strain rate is high. This deformation pattern is a good indicator of the change in plastic properties at the surface of the secondary

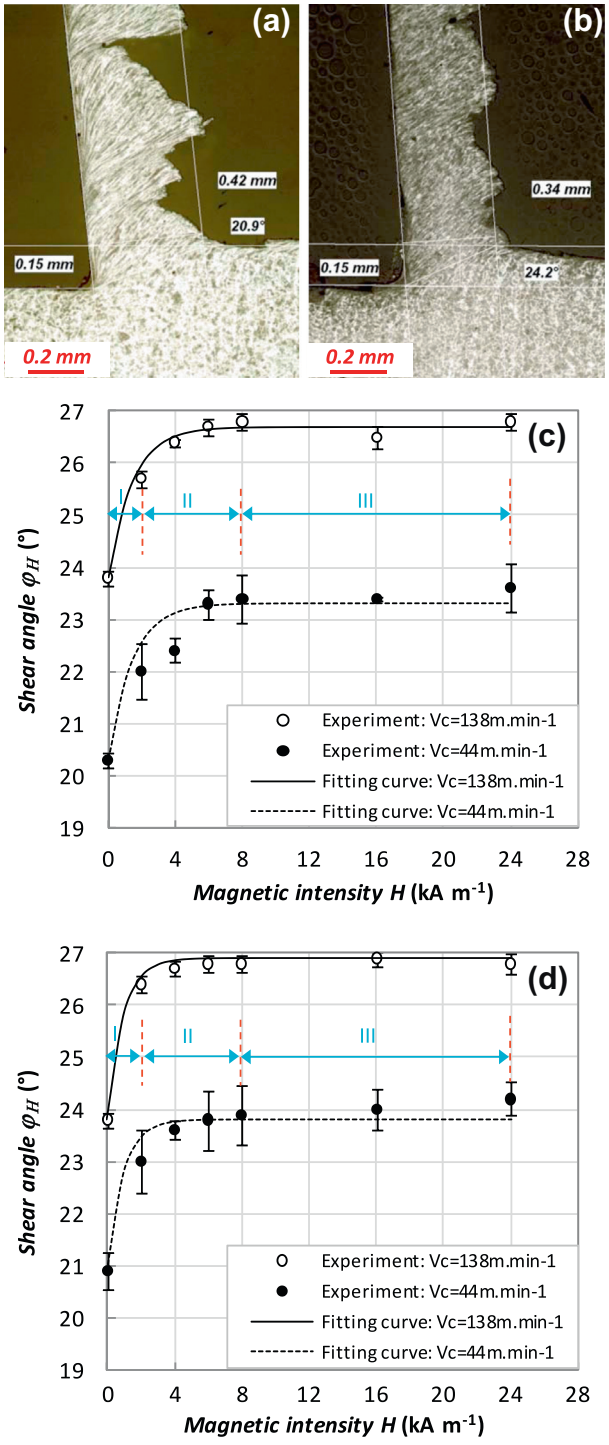

Fig. 2. Typical chip roots obtained by QST (f = 0.15 mm rev^{-1}, V_c = 44 m min^{-1}) for: (a) H = 0 kA m^{-1}, and, (b) H = 24 kA m^{-1}, and, shear angle φ_H vs. magnetic field intensity obtained for: (c) f = 0.10 mm rev^{-1}, and (d) f = 0.15 mm rev^{-1}.

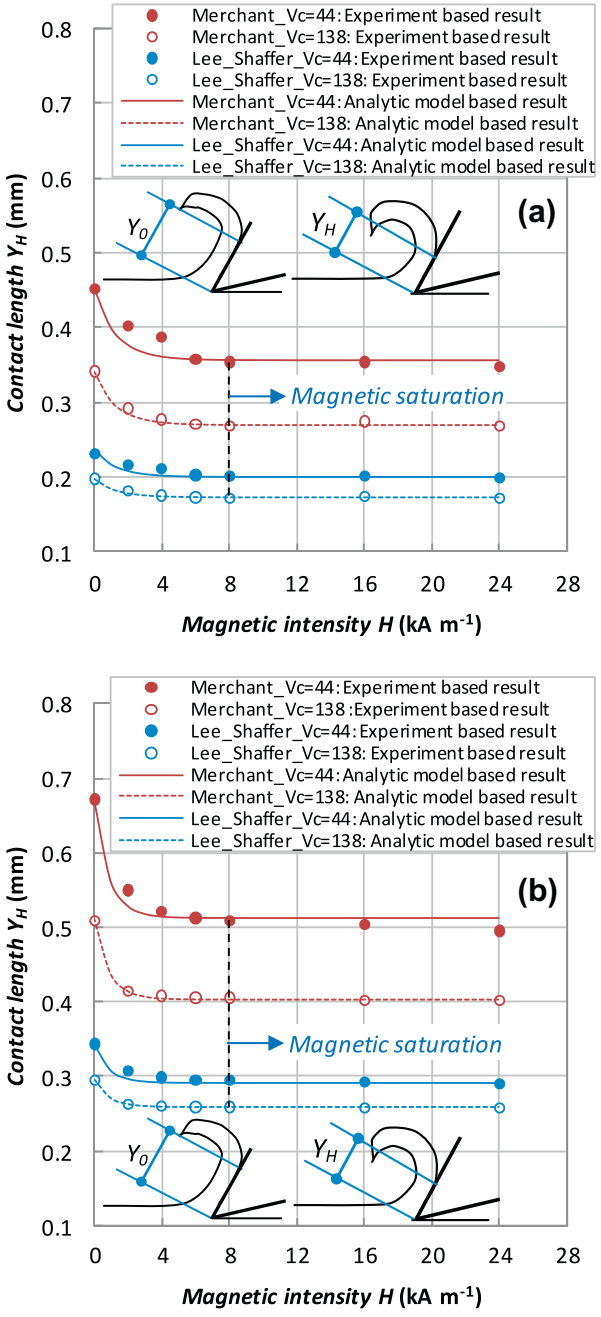

Fig. 3. Contact length vs. magnetic field intensity. (a) f = 0.10 mm rev^{-1}, and (b) f = 0.15 mm rev^{-1}.

layer. The phenomenon is synergetically achieved by two mechanisms: (i) enhanced dislocation number and motion, and (ii) over-delivered heat quantity.

5.2.2. Coefficient of friction

Referring to the constitutive equations coupled with the magnetic field, the friction angle λ_H was deduced by introducing the measured shear angle values in Eqs. (12a) and (12b). From the experimental findings, the magnetic field substantially reduces the friction angle. This observation is valid for both the Merchant and Lee–Shaffer approaches. The secondary shear zone along the line OB can be confused with a boundary layer that is formed as a fluid is forced to flow over a flat plate. Physically, the effect of the magnetic field manifests by the depinning of dislocations from obstacles, which enhances their motions into metals and offers them more mobility in an instable state. This non-equilibrium situation causes a type of instantaneous and local softening along the tool–chip contact surface and should facilitate the formation of the chip against the tool-tip. Thus, the chip will flow much easier over the tool rake face due to better sliding conditions at the interfaces. However, it was found that when the intensity passes from 0 to 24 kA m^{-1}, λ_H decreases by approximately 11% for both the Merchant and Lee–Shaffer models. The drop in the friction angle λ_H (Eqs. (12a) and (12b)) by the relative quantity φ_B partially describes the tribological changes at the secondary surface layer.

Characterizing the contact between the tool and the job surface remains a main problem to overcome in cutting. As is known, the cutting operation requires strong mechanical work that depends on more than one tribological parameter. The delivered work is almost completely converted to heat. Thus, tribological

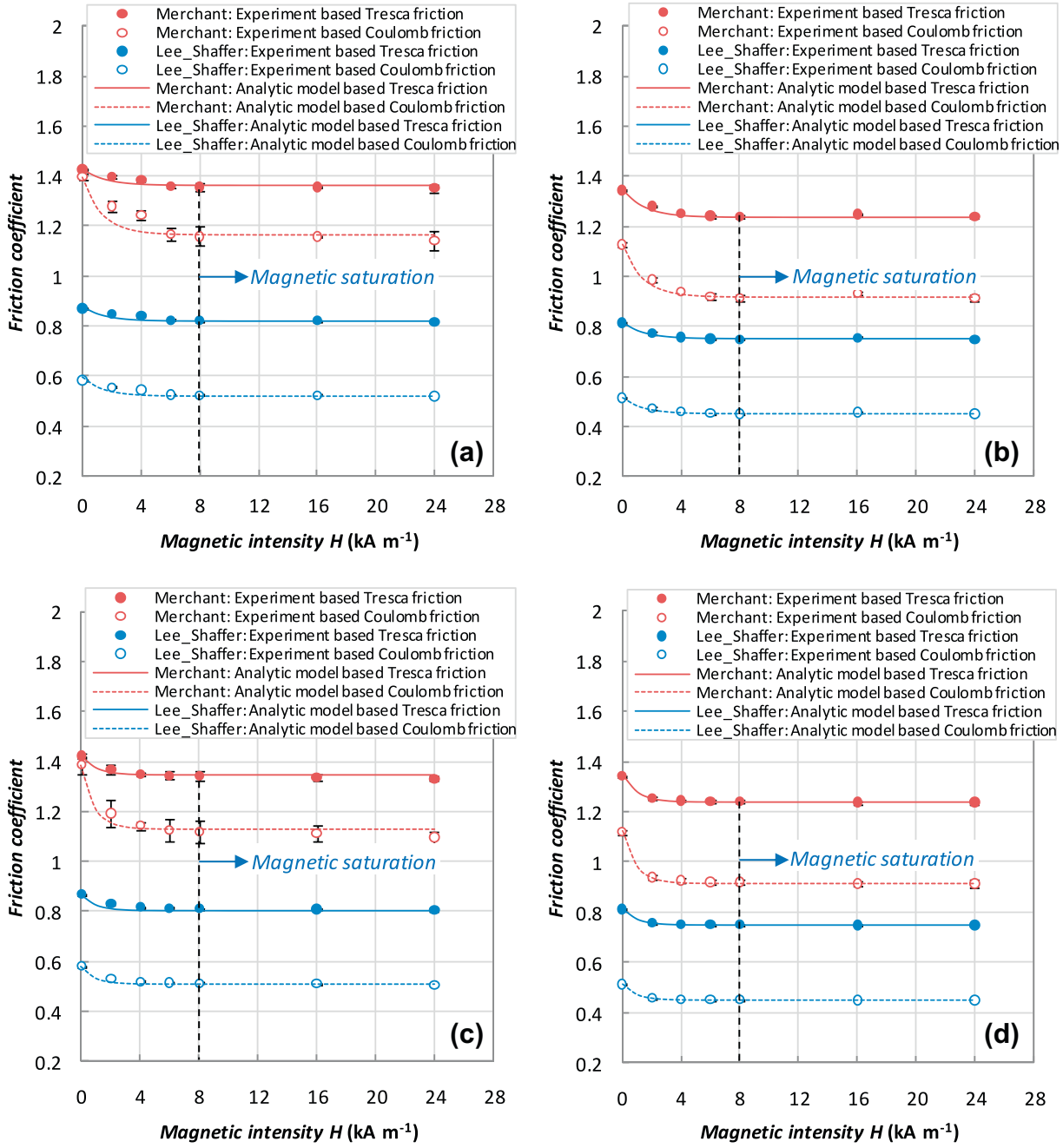

Fig. 4. Coulomb- and Tresca friction coefficients vs. magnetic field intensity. (a) $f = 0.10$ mm rev^{-1}, $V_c = 44$ m min^{-1}, (b) $f = 0.10$ mm rev^{-1}, $V_c = 138$ m min^{-1}, (c) $f = 0.15$ mm rev^{-1}, $V_c = 44$ m min^{-1}, and (d) $f = 0.15$ mm rev^{-1}, $V_c = 138$ m min^{-1}.

factors play a main role in the material removal mechanisms. Controlling those factors requires great care in defining the tool coating type, speed, lubricant characteristics, etc. However, tool wear and failure are inevitable because of severe operating conditions. Today, the common engineering solutions for overcoming some of the difficulties are based either on optimizing the cutting conditions or on using wear-resistant coatings. The friction coefficient analyses in magnetically assisted cutting are found to be very encouraging.

Fig. 4 depicts the evolution of friction coefficients computed using both the measured values and the analytical shear angle values (φ_H). The coupled equations established for Merchant and Lee–Shaffer were used to estimate the friction according to both the Tresca and Coulomb theories. The obtained curves show good agreement between the analytical predictions and the results based on the measurements. Clearly, the friction coefficient decreases due to a decrease in the friction angle λ_H. The friction value decreases as the magnetic intensity increases and the saturation domain is approximated. In spite of the dry cutting, friction markedly decreases when the tool operates in a magnetized environment. Comparing the friction values obtained from magnetically free cutting and magnetically assisted cutting at the saturation domain reveals that the Merchant formulation leads to a higher variation gap than the Lee–Shaffer formulation for all speed–feed rate combinations used.

From the open literature (Merchant, 1945a,b), friction values estimated using the conventional Merchant model are higher than those evaluated by that of Lee–Shaffer. This observation also applies to the coupled models. Regarding the obtained results, operating in the presence of a magnetic field should ultimately lead to reducing friction at the interfaces until saturation is reached.

From the first stage of the tool engagement in the material, the surface state of the secondary zone is subjected to hard deformation mechanisms. The changes to which the material behavior is subjected in such a zone are considered among the principal mechanisms that govern the contact. As previously mentioned, plasticity is affected due to the magnetic excitation and, consequently, the tool will operate in much less severe conditions. This can be attributed to two actions. The first is a *mechanical* action resulting in the decrease of feed force because of the addition of a magnetic force component that acts to repel the tool from the job surface. The force diagram changes alter the tribological characteristics at the interfaces in such a manner to decrease the force ratio $\left(\frac{F_t}{F_n}\right)$ to $\left(\frac{F_{tH}}{F_{nH}} = \frac{F_{aH}}{F_{cH}}\right)$. The second is a *physical* action resulting in a plasticity enhancement due to the increased dislocation motion arising from magnetization, which induces transformations in the material behavior. This helps the tool to operate in more favorable conditions such as low friction.

6. Conclusions

The validity of the approach proposed in this study offers an alternative to assessing the modifications in tribological mechanisms when using magnetically assisted dry cutting. The shear angle law is derived with respect to the magnetic steel behavior. From the obtained results, the following conclusions can be drawn:

- The analysis of the chip formation process proved that a magnetic intensity alters the plastic shear mechanisms within the primary zone to increase the shear angle by approximately $2.975 \pm 0.095^\circ$ irrespective of the cutting conditions.
- The coupled magnetic–mechanical constitutive approach built using the Merchant and Lee–Shaffer classic models showed an ability to predict the cutting behavior in magnetized environments.
- The predictions of contact length and friction coefficient are very encouraging because they showed a good agreement with the results based on the measurements. It was found that both the contact length and friction increasingly fall with the magnetic intensity up to the saturation domain. Therefore, such assistance for cutting might seriously reduce tool wear and, accordingly, improve its lifetime.

Acknowledgments

The authors are grateful to Mr. R. GOERGLER and J. VOISIN for their assistance in improving the quick-stop device and for much help with the experimental procedure.

References

Al'shits, V.I., Darinskaya, E.V., Kazakova, O.L., Mikhina, E.Y., Petrzhik, E.A., 1994. Magnetoplastic effect in non-magnetic crystals and internal friction. J. Alloy. Compd. 211–112, 548–553.

Al'shits, V.I., Darinskaya, E.V., Kazakova, O.L., Mikhina, E.Y., Petrzhik, E.A., 1997. Magnetoplastic effect in nonmagnetic crystals. Mat. Sci. Eng. A 234–236, 617–620.

Åstrand, M., Selinder, T.I., Fietzke, F., Klostermann, H., 2004. PVD-Al_2O_3-coated cemented carbide cutting tools. Surf. Coat. Tech. 188–189, 186–192.

Bagchi, P., Ghosh, A., 1971. Mechanism of cutting tool wear in the presence of magnetic field. Indian J. Technol. 9, 165–169.

Balint, D.S., Descpande, V.S., Needleman, A., Van Der Giessen, E., 2008. Discrete dislocation plasticity analysis of the grain size dependence of the flow strength of polycristals. Int. J. Plast. 24, 2149–2172.

Bataineh, O., Klamecki, B.E., Koepke, B.G., 2003. Effect of pulsed magnetic treatment on drill. J. Mater. Process. Tech. 134, 190–196.

Chin, K.J., Zaidi, H., Nguyen, M.T., Renault, P.O., 2001. Tribological behavior and surface analysis of magnetized sliding contact XC 48 steel/XC 48 steel. Wear 250, 470–476.

Chin, K.J., Zaidi, H., Mathia, T., 2005. Oxide film formation in magnetized sliding steel/steel contact – analysis of the contact stress field and film failure mode. Wear 259, 477–481.

El Mansori, M., Schmitt, M., Paulmier, D., 1998. Role of transferred layers in friction and wear for magnetized dry frictional applications. Surf. Coat. Tech. 108–109, 479–483.

El Mansori, M., Paulmier, D., 1999. Effects of selective transfer on friction and wear of magnetised steel–graphite sliding couples. Appl. Surf. Sci. 144–145, 233–237.

El Mansori, M., Pierron, F., Paulmier, D., 2003. Reduction of tool wear in metal cutting using external electromotive sources. Surf. Coat. Tech. 163–164, 472–477.

El Mansori, M., Iordache, V., Seitier, P., Paulmier, D., 2004. Improving surface wearing of tools by magnetization when cutting dry. Surf. Coat. Tech. 188–189, 566–571.

El Mansori, M., Mkaddem, A., 2007. Surface plastic deformation in dry cutting at magnetically assisted machining. Surf. Coat. Tech. 202, 1118–1122.

Galligan, J.M., 1982. Electron and phonon drag on mobile dislocations in metals at low temperature. In: Mason, W.P., Thurston, R.N. (Eds.), Physical Acoustics: Principles and Methods, vol. 16. Academic Press, New York, pp. 173–215.

Jaspers, S.P.F.C., Dautzenberg, J.H., 2002a. Material behaviour in metal cutting: strains, strain rates and temperatures in chip formation. J. Mater. Process. Tech. 121, 123–135.

Jaspers, S.P.F.C., Dautzenberg, J.H., 2002b. Material behaviour in conditions similar to metal cutting: flow stress in the primary shear zone. J. Mater. Process. Tech. 122, 322–330.

Kim, C.S., Galligan, J.M., 1992. Influence of viscosity on the escape rate from metastability – creep at low temperature. Acta Metall. Mater. 40, 1187–1194.

Kravchenko, V.Y.A., 1970. Influence of the magnetic field on electronic deceleration of dislocations. J. Exp. Theor. Phys. Lett. 12, 391–393.

Lee, E.A., Shaffer, B.W., 1951. The theory of plasticity applied to a problem of machining. J. Appl. Mech. 18, 405–413.

Merchant, M.E., 1945a. Mechanics of the metal cutting process. I. Orthogonal cutting and a type 2 chip. J. Appl. Phys. 16, 267–275.

Merchant, M.E., 1945b. Mechanics of the metal cutting process. II. Plasticity conditions in orthogonal cutting. J. Appl. Phys. 16, 318–324.

Mkaddem, A., El Mansori, M., 2012. Extension of the slip band area under magnetization during steel machining. Mater. Manuf. Process. 27, 1073–1077.

Molotskii, M., Fleurov, V., 1996. Work hardening of crystals in a magnetic field. Philos. Mag. Lett. 73, 11–15.

Molotskii, M., Fleurov, V., 1997. Manifestations of hyperfine interaction in plasticity. Phys. Rev. B 56, 10809–10811.

Molotskii, M., Fleurov, V., 2000. Dislocation paths in a magnetic field. J. Phys. Chem. B104, 3812–3816.
Singh, S., Shan, H.S., Kumar, P., 2002. Wear behavior of materials in magnetically assisted abrasive flow machining. J. Mater. Process. Tech. 128, 155–161.
Zaidi, H., Senouci, A., 1999. Influence of magnetic field on surface modification and the friction behavior of sliding couple aluminium/XC 48 steel. Surf. Coat. Tech. 120–121, 653–658.